XVI International Conference on Computational Plasticity. Fundamentals and Applications
COMPLAS 2021
E. Oñate, D. Peric, M. Chiumenti and Eduardo de Souza Neto (Eds)

PERFORMANCE OF DIFFERENT CONSTITUTIVE SOIL MODELS: FROM ELEMENT TESTS TO THE SIMULATION OF VIBRATORY PILE DRIVING TESTS

J. Machaček[*,†,‡], P. Staubach[†], M. Tafili[†], H. Zachert[‡] AND T. Wichtmann[†]

[†] Ruhr University Bochum, Department of Civil and Environmental Engineering, Chair of Soil Mechanics, Foundation Engineering and Environmental Geotechnics, Germany

[‡] Technical University of Darmstadt, Department of Civil and Environmental Engineering, Institute of Geotechnics, Germany

[*] e-mail: jan.machacek@tu-darmstadt.de

Key words: Constitutive models, Vibratory pile driving, Fully coupled simulation, Model test, Automatic parameter calibration

Abstract. The present study deals with the investigation of the applicability (by means of parameter calibration), robustness and prediction quality of advanced constitutive soil models for the numerical investigation of complex geotechnical problems. The range of available constitutive soil models extends from simple linear to time-dependent and hydromechanically coupled nonlinear modelling approaches. It is the user's task to select a constitutive model suitable for the problem at hand. This requires in-depth knowledge of the soil behaviour as well as the strengths and weaknesses of the available constitutive models, most of which have only been validated using element test simulations. The procedure from parameter calibration using laboratory tests under well-defined boundary conditions (element tests) to the simulation of boundary value problems is complex in many respects and is often not followed with advanced constitutive models due to the large number of parameters required and the necessary laboratory tests. In this paper, the prediction quality of three models, namely Hypoplasticity with Intergranular Strain, Sanisand and Hypoplasticity with Intergranular Strain Anisotropy is inspected. The investigation is carried out based on back-calculations of laboratory tests and a well-documented model test to evaluate their suitability in representing complex soil mechanical aspects, such as the material behaviour under cyclic loading, particularly pore pressure accumulation. The parameter calibration is performed both "manually" as well as with a specially developed automatic calibration software. Subsequently, model tests of vibratory pile driving in water-saturated sand are simulated using the previously calibrated parameters.

1 INTRODUCTION

The numerical simulation of geotechnical structures often requires the use of sophisticated constitutive soil models, especially when the investigated structure is subjected to cyclic loading. These constitutive models should accurately represent the mechanical

behaviour of soil under different stress and strain amplitudes, including the accumulation of pore water pressure in undrained or partially drained conditions and cyclic mobility effects. Complexity of advanced constitutive models grows significantly as a result of addressing these effects. Besides the void ratio-, pressure-, and time-dependence of the soil behaviour and the anisotropy of some soil types, the main challenge has been to reproduce the specific soil behaviour under cyclic loading. As a result, different mechanisms have been incorporated into different families of constitutive models, such as history variables/surfaces and their evolution laws in elastoplastic frameworks [4, 1] or the intergranular strain concept incorporated in hypoplastic models [14, 5], amongst others. Various constitutive models coexist today and modifications, extensions, and new formulations are proposed regularly. However, due to the complexity of the models, performance checks are often only conducted based on element tests, see for instance [4, 13, 21, 19].

A comparison of the prediction quality in boundary value problems (BVPs) is often missing but attracting growing interest, see e.g. [9, 15]. It is not surprising that the assessment was absent, since simulations of BVPs require very thorough implementations of the soil models to ensure sufficient numerical stability and robustness. As a result of the requirement for robustness, (undocumented/uncommunicated) minor modifications of the constitutive model are often necessary as well as detailed expertise. In this context, we refer to [11] for modifications of the constitutive models used in this work.

Furthermore, these advanced constitutive models often require lengthy and complex parameter calibration procedures involving a large number of tailored laboratory tests. In this work, three sophisticated constitutive models are compared: Hypoplasticity with two different extensions, the Intergranular Strain (*Hypo+IGS*) extension and Intergranular Strain Anisotropy (*Hypo+ISA*) extension as well as the *Sanisand* model. Due to the large deformations during the pile penetration studied as BVP in this work, an updated Lagrangian formulation is employed.

One of this paper's objectives is to demonstrate that a parameter calibration for the models at hand can be based on a few well chosen laboratory tests to reach a satisfactory prediction of advanced BVPs. Moreover, one additional parameter set for the *Hypo+IGS* model has been calibrated using a newly developed automated calibration software developed by the first author. It will be shown, that the automatically calibrated parameters perform at least equivalent to the ones calibrated "by hand", while enabling a significantly less time-consuming calibration process and, in particular, a significant reduction in application hurdles when using advanced constitutive soil models.

2 VIBRATORY PILE DRIVING MODEL TESTS

The vibratory pile driving model tests have been performed by J. Vogelsang in Karlsruhe and are reported in [20]. A schematic sketch, a photo showing the front of the container with marked positions of the pore pressure transducers (PPT) and a view from above are given in Fig. 1a), b), c). In the symmetry axis, an acrylic front pane has been attached, which serves as an observation window during the experiments. Along the pane, the model piles were inserted displacing the soil. To prevent deflections of the acrylic front pane, stiffening beams were added from the outside. A watertight connection of the

individual segments allows the tests to be performed in water saturated soil.

The vibration-generating driving unit was bolted to the pile head in a free-riding manner. A load cell between vibrator and pile measured the force during the driving process. The experiments were thus performed force- and not displacement-controlled. A frequency of $f = 25$ Hz with a static moment of the vibrator of $M_{stat} = 5.33 \cdot 10^{-3}$ kg·m has been used. The aluminium pile had a diameter of $d_{Pile} = 33$ mm and a 60° pointed tip. The combined mass of the pile, the load cell and the vibrator was $m_{vib} = 7.881$ kg.

For the test considered in the numerical back-analysis, the soil height was 0.81 m and the initial relative density $D_{r0} = 0.71$. In order to ensure nearly water-saturated conditions, dry so-called "Karlsruhe Sand" was pluviated into the model container filled with deaerated water. The water table has been set level with the soil during the pile penetration process.

The index parameters of "Karlsruhe Sand" are: median grain size $d_{50} = 0.55$ mm, coefficient of uniformity $C_U = 1.53$, grain density $\rho^s = 2.65$ g/cm^3, minimum void ratio $e_{min} = 0.549$ and maximum void ratio $e_{max} = 0.851$. The hydraulic conductivity k for "Karlsruhe Sand" was determined experimentally with different soil densities in order to estimate k for a given porosity n using the Kozeny/Carman equation [10, 3]:

$$k(n) = \frac{1}{C}\frac{\gamma^w}{\eta^w}\frac{n^3}{(1-n)^2}d_e^2. \tag{1}$$

Therein, $\gamma^w = 10$ kN/m^3 is the dead weight and η^w the dynamic viscosity of the pore water. The effective grain size of "Karlsruhe Sand" is $d_e = 0.5$ mm and $C = 308$ [20].

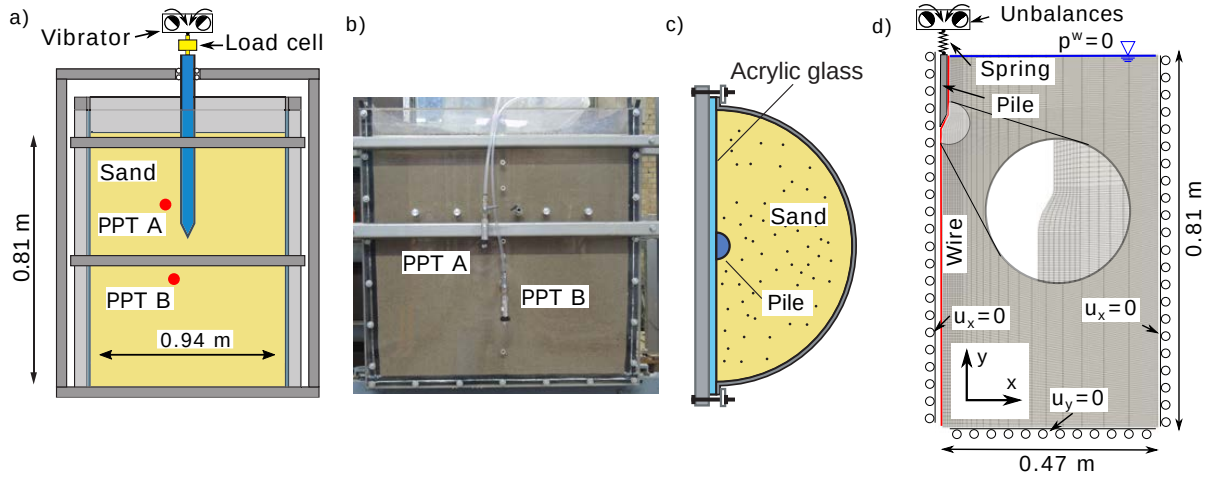

Figure 1: Schematic illustration of the test device a) and picture of the device b) with the already embedded soil. A view from above is given in figure c). The pore pressure transducers (PPT) are marked according to their location (not scaled, based on [20]). The finite element model adopted for the simulation of the test is provided in figure d).

3 NUMERICAL MODEL FOR THE BACK-ANALYSIS

The finite element code `numgeo`[1] has been used for the simulation of the model tests. The implementations of *Hypo+IGS*, *Sanisand* and *Hypo+ISA* in `numgeo` as described in [11] have been utilised. The numerical model adopted for the simulation of the vibratory pile driving tests is depicted in Fig. 1d). The numerical model has been discretised using approximately 4000 elements. Quadratically interpolated **u**-p elements (see [23]) have been used to discretise the soil. The **u**-p element formulation neglects the relative acceleration between the solid and the water phase and its applicability can be challenged in case of wave propagation with high frequency and simultaneously high hydraulic conductivity. In a preceding study [16], the influence of different element formulations on the simulation results for the problem at hand was investigated. It was found that there was little difference in the results for the various element formulations, and that the **u**-p formulation is appropriate for the simulation of vibratory pile driving. Considering that the numerical model is axisymmetric and the experiments have been conducted on half of an axisymmetric physical model, the masses and forces of the pile-vibrator system were scaled accordingly.

The zipper-method is used to avoid mesh distortion during the pile penetration process. This method has been used in [2, 6] as well and makes the application of large-deformation techniques such as the MPM or Eulerian based schemes obsolete for the problem at hand. As is reported in [18], the application of a Coupled Eulerian-Lagrangian technique for the simulation of the vibratory pile driving tests gives similar results as the zipper-method but adds considerable numerical complexity. Using the zipper-method, the boundary of the soil in the symmetry axis below the pile tip is not constraint by Dirichlet boundary conditions in horizontal direction but by a contact constraint with a thin vertical extension of the pile directly in the symmetry axis (see red line in Fig. 1d)).

As in the experiments, a load cell between the pile and the imbalance, as well as the imbalance itself on top is considered in the numerical model (idealised as mass points). As illustrated in Fig. 1d), the solid displacements are constrained perpendicular to the bottom, left, and right boundaries. All contact surfaces are discretised using a surface-to-surface approach (see e.g. [22] for details). The penalty method is used to enforce the contact conditions in the normal direction. Friction between the aluminium pile and the soil is modelled using a Coulomb friction model. The normal contact between pile and soil is assumed to be inseparable, as water cannot separate from the pile, provided no cavitation occurs. Accounting for minor air inclusions caused by the sand pluviation process, a degree of saturation $S \geq 0.999$ is assumed. Using the initial porosity of the soil, the bulk modulus of the pore water is $\bar{K}^w = 1.2 \cdot 10^4$ kPa.

4 PARAMETER CALIBRATION

Prior to the simulation of the vibratory pile driving tests, the constitutive parameters of the sand used in the experiment ("Karlsruhe sand") had to be determined for each

[1] `numgeo` (see [12, 11, 17] and `www.numgeo.de`) is an in-house finite-element program, developed by the first two authors for the solution of non-linear, coupled (dynamic) geotechnical boundary value problems.

constitutive model. Experiments used for calibration of the material parameters are two oedometric compression tests (initially loose $D_{r0} = 0.13$ and dense $D_{r0} = 0.96$ samples) with loading, unloading and reloading, drained monotonic triaxial tests (on samples with varying initial relative densities) with initial mean effective stress $p_0 = 20$ kPa and $p_0 = 100$ kPa and one undrained triaxial test with strain cycles of amplitude $\varepsilon^{ampl} = 0.05$ (medium dense $D_{r0} = 0.60$ sample). One set of parameters has been calibrated "by hand" for each constitutive model, as stated in the introduction. Details on this calibration procedure are provided in [11].

Additionally, a second set of parameters was calibrated for the Hypo+IGS model using an automatic calibration (AC) tool developed by the first author. The automatic calibration program aims to simplify and speed up the calibration process and, in particular, to reduce the application hurdles when using advanced constitutive soil models. In addition, this program helps to reduce the "human factor" in the calibration of model parameters (e.g., subconscious personal preferences, outcome-based calibrations and experience of the person performing the calibration). At its heart, the automatic calibration program combines the finite-element program `numgeo`[1], with the optimisation functionalities implemented in Python's scipy [8]. This allows an easy import of all test data and the subsequent automatic calibration with the identical implementation of the constitutive model which is also used for the simulation of boundary value problems. In the present case, for the Hypo+IGS model, the automatic calibration tool estimates an initial set of parameters based on the procedure proposed by Herle [7]. This parameter set is subsequently iteratively improved by minimising a scalar error function. For this purpose, various minimisation strategies are available via Python's scipy. In the present case, a nesting of a basin-hopping algorithm with a Constrained Optimisation BY Linear Approximation (COBYLA) algorithm was used. The error function used for the optimisation is defined as follows:

$$\epsilon = \sum_{i}^{n} w^i \epsilon^i = \left(w^{oed}\epsilon^{oed} + w^{CD}\epsilon^{CD} + w^{CUc}\epsilon^{CUc} \right) \tag{2}$$

with the weighting factors w^i and the error functions ϵ^i of the oedometric compression tests ($i = oed$), the drained monotonic ($i = CD$) and undrained cyclic triaxial tests ($i = CUc$), respectively. In the present case $w^i = 1/3$ was used, i.e. all three types of laboratory tests were equally weighted. The error functions have been developed with the aim of taking into account the basic characteristics of the various laboratory tests, thus mimicking the approach of an experienced engineer calibrating the model based on the basic characteristics of the laboratory tests. Different functions are conceivable for this. Based on the authors' experience, the following definitions have proven themselves suitable so far and were also used in this work:

$$\epsilon^{oed} = \sum_{t=1}^{n^t} \sqrt{\sum_{i=1}^{n^{inc}} \left(\frac{\Delta\varepsilon_i^{exp} - \Delta\varepsilon_i^{sim}}{\Delta\varepsilon_i^{exp}} \right)^2} \tag{3}$$

$$\epsilon^{CD} = \sum_{t=1}^{n^t} \sqrt{\sum_{i=1}^{n^{inc}} \left(\frac{q_i^{exp} - q_i^{sim}}{q_i^{exp}} \right)^2} \tag{4}$$

$$\epsilon^{CUc} = \sum_{t=1}^{n^t} \sqrt{\sum_{i=1}^{n^{inc}} \left(\frac{\Delta p_i^{w,exp} - \Delta p_i^{w,sim}}{\max(\Delta p^{w,exp})} \right)^2 + \sum_{i=1}^{n^{inc}} \left(\frac{q_i^{peak,exp} - q_i^{peak,sim}}{\max(q^{peak,exp}) \cdot i} \right)^2} \tag{5}$$

Therein, $\sum_{t=1}^{n^t}$ denotes the sum over all tests (of one experiment type) and $\sum_{i=1}^{n^{inc}}$ is the sum over all load increments (by means of prescribed stress in load controlled tests and prescribed strains/displacements in strain controlled tests) for the oedometric compression and the drained triaxial tests. For cyclic triaxial tests, $\sum_{i=1}^{n^{inc}}$ is the sum over all applied load cycles. From Eq. (3) it can be seen that for the oedometer test the error is evaluated based on the strain increment $\Delta\varepsilon$ caused by a prescribed load increment. For the stress controlled drained monotonic triaxial test (Eq. (4)), the deviation between the experiment and the simulation is judged by means of the second Roscoe invariant q. For the undrained cyclic triaxial test, two criteria are used to assess the quality of the recalculation: the agreement of the accumulated pore water pressure Δp^w per cycle and the maximum/minimum deviatoric stress q^{peak} reached per cycle. By introducing the cycle number i in the denominator of the second fraction of Eq. (5), an automatic weighting is performed: Deviations in the first cycles are penalised more strictly than deviations after a large number of load cycles.

The results of the calibration are provided by means of comparison of experimental and numerical data for the oedometric compression tests in Fig. 2, for the drained monotonic triaxial tests in Fig. 3 and the undrained cyclic triaxial test in Fig. 4, respectively. *Hypo+IGS (AC)* denotes the parameter set determined by means of automatic calibration. The parameters for the different constitutive models are summarised in Table 1. Note that for the *Hypo+IGS (AC)* and the *Hypo+ISA* models only the parameters differing from the *Hypo+IGS* model are provided.

Hypo+IGS

φ_c	h_s	n	e_{d0}	e_{c0}	e_{i0}
33.1°	19 GPa	0.285	0.549	0.851	0.979

α	β	m_T	m_R	R	β_R	χ
0.1	0.32	1.2	2.4	$5 \cdot 10^{-5}$	0.08	7

Hypo+IGS (AC)

differing from *Hypo+IGS*:	h_s	n	β
	9.2 GPa	0.32	0.671

m_T	m_R	β_R	χ
2.24	1.77	0.09	13.05

Hypo+ISA

differing from *Hypo+IGS*:	β	m_R
	2.5	3

β_R	χ_0	χ_{max}	C_a
0.28	7	8	0.012

Sanisand

p_a	e_0	λ_c	ξ	M_c	c	m	G_0
100 kPa	1.1	0.25	0.35	1.3	0.88	0.05	70.0

ν	h_0	c_h	n_b	A_0	n_d	$z_{\max}$	c_z
0.05	8.0	0.35	1.3	0.8	0.8	60.0	2000

Table 1: Summary of constitutive model parameters for the *Hypo+IGS*, *Sanisand* and *Hypo+ISA* model

For the oedometric compression tests, all constitutive models show a poor performance during reloading for both loose and dense conditions since the reloading stiffness is strongly underestimated. The overall best agreement is achieved with the automatically calibrated

parameter set *Hypo+IGS (AC)*. From the simulations of the drained monotonic triaxial tests (see Fig. 3), one may note that the peak strength is noticeably underestimated by the *Sanisand* model, while the hypoplastic models tend to overestimate the peak strength. For dense samples, the *Hypo+ISA* model overestimates the residual strength noticeably. For the loose sample and the sample with $p_0 = 20$ kPa all three models show a good agreement with the experimental results. The evaluation of the effective stress paths of the undrained cyclic triaxial test depicted in Fig. 4 shows a good performance of the hypoplastic models. Contrarily, the *Sanisand* simulation underestimates severely the deviatoric stress in both triaxial compression and extension. All models reproduce the build-up of excess pore water pressure Δp^w during the first 10 cycles as well as the final value of Δp^w which is identical to the initial mean effective stress p_0. However, for $N > 10$, the rate of pore water pressure build-up is significantly overestimated in the simulations with the *Hypo+IGS*, *Hypo+ISA* and *Sanisand* model. In terms of rate of pore water pressure build-up, the *Hypo+IGS (AC)* simulation shows the best agreement with the experimental results. An in-depth

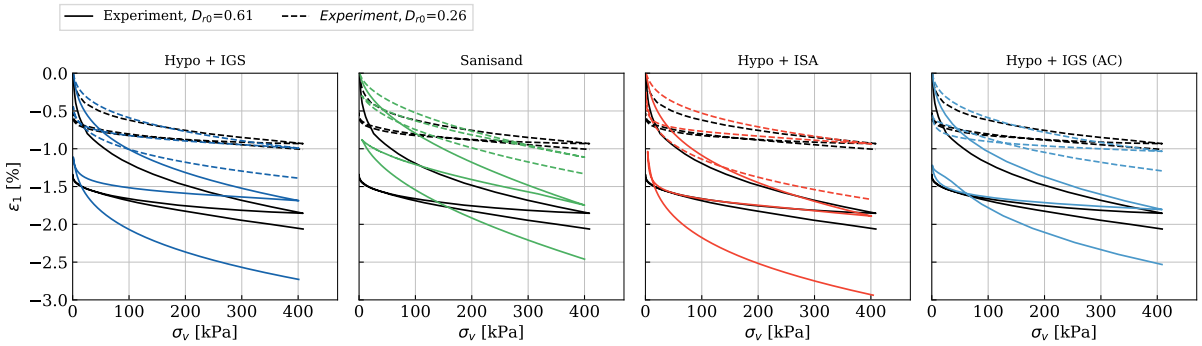

Figure 2: Comparison of oedometric compression test results (black lines) with corresponding simulations (coloured lines) on one loose and one dense sample.

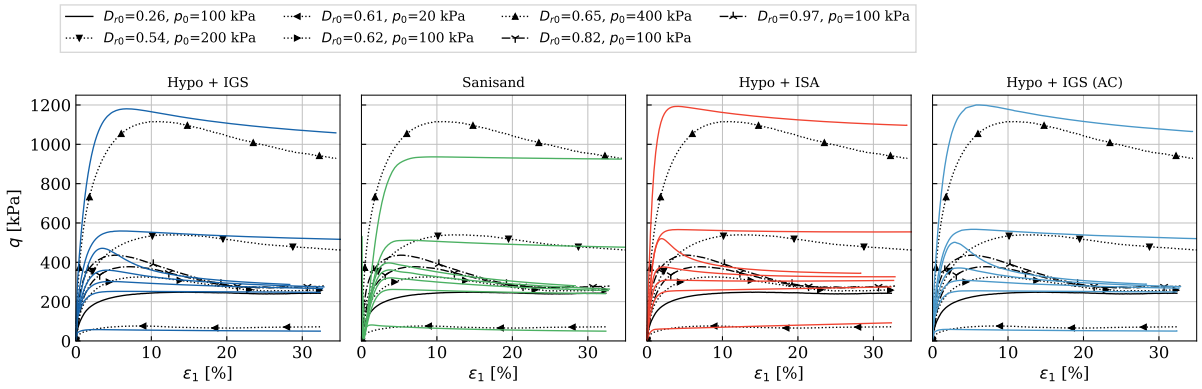

Figure 3: Experimental results (black lines) and simulations (coloured lines) of drained monotonic triaxial tests on samples with different densities and different initial pressures.

discussion of the simulation results is given in [11].

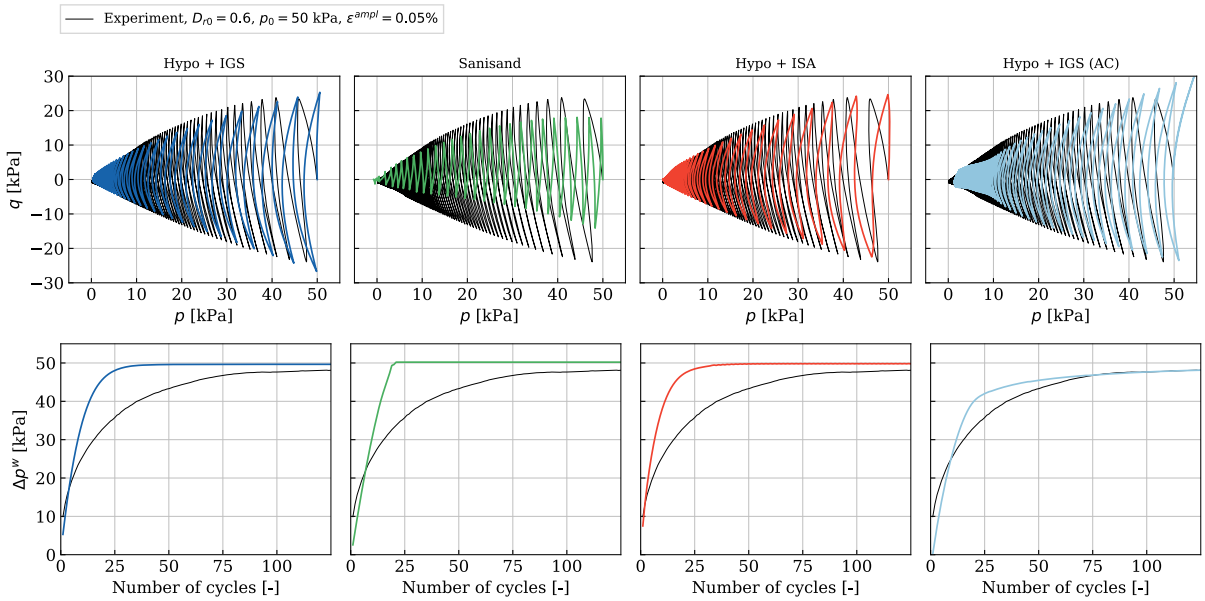

Figure 4: Experiment (black) and simulations (coloured lines) of an undrained cyclic triaxial test on a medium dense sample with isotropic consolidation and strain cycles.

5 COMPARISON BASED ON VIBRATORY PILE DRIVING TESTS

In the following, the capabilities of the chosen numerical approach in combination with the three constitutive models for the back-calculation of the model test are investigated. The examination of the results includes comparisons of the pile displacements (Fig. 5), the pore pressure development at two different locations (Fig. 6) and the development of pile force vs. pile penetration (Fig. 7). Supplementary comparisons including contour plots of incremental vertical and horizontal displacements in the vicinity of the pile, acceleration-time histories and detailed examinations of the pile force vs. pile penetration relationship for individual cycles can be found in [11]. The development of the normalised pile displacement $\tilde{u}_y$ during the vibration is depicted in Fig. 5. The overall trend as well as the magnitude of pile displacement are reproduced well by all simulations. Especially with regard to the complexity of the experiment, these results are judged as satisfactory. However, some discrepancies are noticed. In spite of the nearly perfect agreement between the simulated and measured pile displacements during the first 3 seconds, the Sanisand model predicts almost constant pile penetration rates (for $t > 3$ s), which is in contrast to the decrease in penetration rate observed in the experiment.

Two pore pressure transducers, PPT A and PPT B, were used to measure changes in pore water pressure. Figure 6 compares the simulation results with measurements for PPT A. Therein, Δp^w denotes the change in pore water pressure and p_0^w is the initial (hydrostatic) pore water pressure. For comparisons for PPT B, the reader is referred to [11].

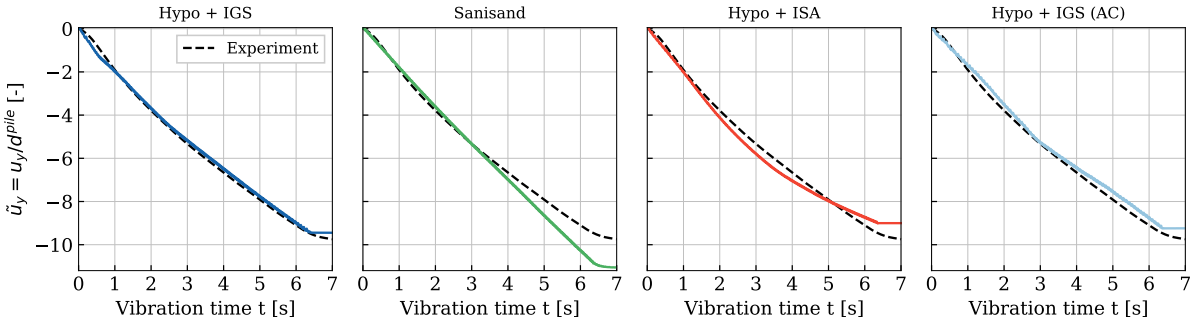

Figure 5: Comparison of normalised pile penetration over vibration time for the experiment (black) and the simulations (coloured).

Referred to the driving process in the experiment, PPT A is passed by the pile tip after the first seconds of vibration. When comparing the measurements of pore water pressure for PPT A to those calculated, despite an overall good agreement, all simulations exhibit different shortcomings. For the simulation with the *Hypo+IGS* model a good agreement of the minimum values of pore water pressure ($\Delta p^w/p_0^w < 0$, i.e. decrease with respect to the hydrostatic values) during vibration is observed. However, the maximum values of pore water pressure (and thus the tendency towards contraction under cyclic loading) during the first two seconds of pile driving are strongly underestimated in the simulation. This disadvantage is not encountered in the simulation with *Hypo+IGS (AC)*. Accordingly, the deficit is not due to the constitutive model, but to the calibrated parameters. The opposite is observed for the simulation with the *Hypo+ISA* model: while the maximum pore water pressure in each cycle is captured satisfactory, the *Hypo+ISA* model fails to reproduce the decrease in pore water pressure and thus does not adequately capture the tendency towards dilatation under cyclic loading. The *Sanisand* model is capable of capturing both positive and negative pore pressure increments in contrast to the hypoplastic models. However, the *Sanisand* simulation drastically overestimates the change in pore

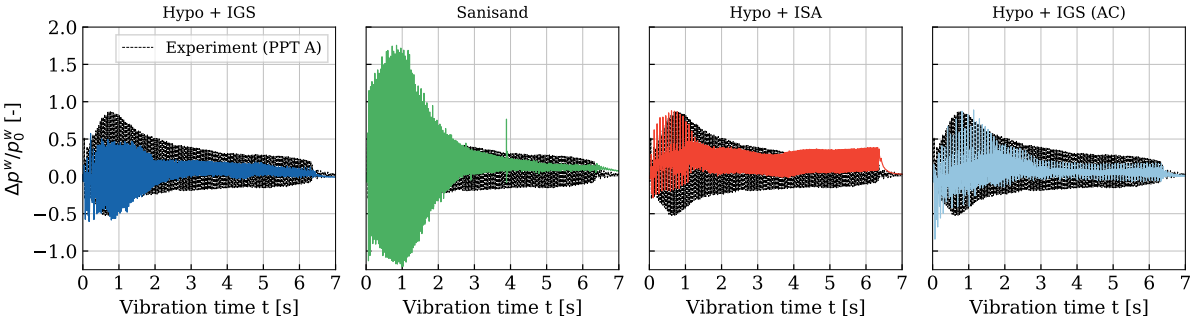

Figure 6: Development of excess pore water pressure recorded at PPT A in the experiment (black) and the simulations (coloured).

water pressure during the first two seconds. All simulations underestimate the amplitude of incremental pore water pressure after the pile tip passes the transducer.

To further evaluate the performance of the different constitutive models, the measured and calculated (normalised) pile force as a function of the normalised pile displacement $\tilde{u}_y$ is compared in Fig. 7. Normalisation ensures comparability between the simulation (full model) and the experiment (nearly half model). The normalised pile force reads: $\tilde{F}^{Pile} = (F^{Pile} - m^{Pile} \cdot a_y^{Pile})/F_{stat}^{Pile}$. Therein, $m^{Pile} \cdot a_y^{Pile}$ is the pile inertia force, F^{Pile} is the head forces (measured between the unbalances and the pile head) and F_{stat}^{Pile} is the static pile force resulting from the dead weight of the pile, the oscillator and the load cell. Both the measured and the calculated pile head force F^{Pile} contain the skin friction as well as the tip resistance. In fact, the development of the pile force in the simulations reflects the mobilised soil resistance during pile driving.

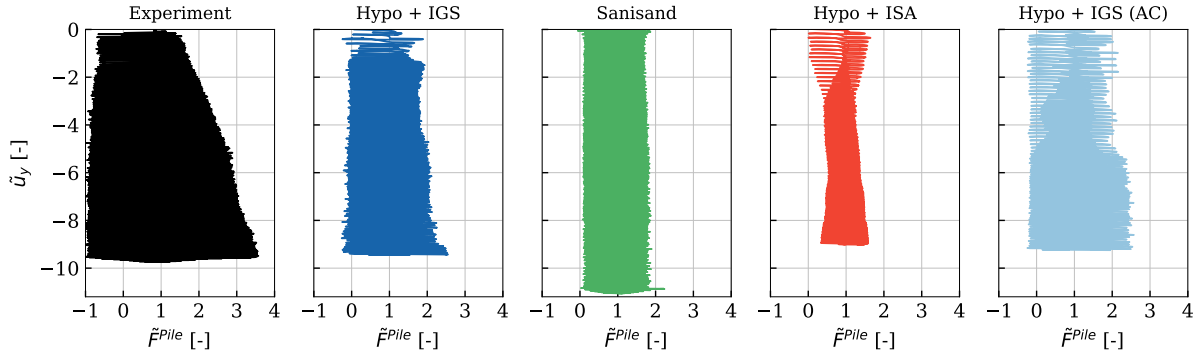

Figure 7: Normalised pile force $\tilde{F}^{Pile}$ as function of the normalised pile displacement $\tilde{u}_y$.

The experiment showed an increase of normalised pile force $\tilde{F}^{Pile}$ (both negative and positive) with increasing pile penetration $\tilde{u}_y$. While the pile force at the beginning of the pile driving is in the range $-0.6 \leq \tilde{F}^{Pile} \leq 1.5$, this range increases with penetration depth until it reaches final values of $-1.0 \leq \tilde{F}^{Pile} \leq 3.5$. The simulated pile forces do not reflect this steady increase, irrespective of the chosen constitutive model or parameter set.

6 CONCLUSIONS

The performance of three constitutive models (*Hypo+IGS*, *Sanisand*, *Hypo+ISA*) was investigated based on the back calculation of laboratory tests (oedometer, monotonic and cyclic triaxial tests) and a vibratory pile driving model test in saturated sand. In addition, first simulations with automatically calibrated parameters for the Hypo+IGS model were presented. The automatic calibration software is based on the same software (`numgeo`) with which the simulation of the vibratory pile driving was performed. In combination with the numerical implementation, all three constitutive models were able to reproduce satisfactorily the pile displacement and gave acceptable predictions of the development of excess pore water pressure during the vibratory driving process. The development of pile

force with increasing pile penetration could not be accurately reproduced by the simulations. The overall best agreement with the experiment was observed for the hypoplastic model with automatically calibrated parameters (*Hypo+IGS (AC)*). In summary, the results of the present study demonstrate that existing advanced constitutive models can be successfully applied in numerical studies of complex geotechnical BVPs. In light of the high frequency cyclic loads applied to saturated soil at small stress states, the investigated BVP places a tremendous demand on the numerical methods and constitutive models. In particular, the cyclic shearing in the contact zone between the pile and the soil requires numerically stable and robust implementations. Future work will focus on including further advanced constitutive models into the comparative study, improving the automatic calibration tool, e.g. by introducing a particle swarm algorithm for the optimisation and testing additional error functions.

References

[1] T. Benz. "Small-strain stiffness of soils and its numerical consequences". PhD thesis. University of Stuttgart, 2007.

[2] P. van den Berg. "Analysis of soil penetration". PhD thesis. Delft University of Technology, 1994.

[3] P. C. Carman. "Permeability of saturated sands, soils and clays". In: *The Journal of Agricultural Science* 29.2 (Apr. 1939), pp. 262–273.

[4] Y. Dafalias and M. Manzari. "Simple plasticity sand model accounting for fabric change effects". In: *Journal of Engineering Mechanics* 130.6 (2004), pp. 622–634.

[5] W. Fuentes and Th. Triantafyllidis. "ISA model: A constitutive model for soils with yield surface in the intergranular strain space". In: *International Journal for Numerical and Analytical Methods in Geomechanics* 39.11 (Mar. 2015), pp. 1235–1254.

[6] S. Henke and J. Grabe. "Numerical investigation of soil plugging inside open-ended piles with respect to the installation method". In: *Acta Geotechnica* 3 (2008), pp. 215–223.

[7] Ivo Herle. *Hypoplastizität und Granulometrie einfacher Korngerüste*. Promotion, Institut für Bodenmechanik und Felsmechanik der Universität Fridericiana in Karlsruhe, Heft Nr. 142. 1997.

[8] Eric Jones, Travis Oliphant, Pearu Peterson, et al. *SciPy: Open source scientific tools for Python*. 2001–.

[9] Hans Petter Jostad et al. "Evaluation of soil models for improved design of offshore wind turbine foundations in dense sand". In: *Géotechnique* 70.8 (Aug. 2020), pp. 682–699.

[10] Josef Kozeny. *Über kapillare Leitung des Wassers im Boden (Aufstieg, Versickerung u. Anwendung auf die Bewässerung)*. Hölder-Pichler-Tempsky, A.-G.[Abt.]: Akad. d. Wiss., 1927.

[11] J. Machaček et al. "Investigation of three sophisticated constitutive soil models: from numerical formulations to element tests and the analysis of vibratory pile driving tests". In: *Computers and Geotechnics* (2021 (accepted 29.05)).

[12] Jan Machaček. "Contributions to the Numerical Modelling of Saturated and Unsaturated Soils". Heft 187, ISSN 0453-3267. PhD thesis. Veröffentlichungen des Instituts für Bodenmechanik und Felsmechanik am Karlsruher Institut für Technologie (KIT), 2020.

[13] David Mašın. "Clay hypoplasticity with explicitly defined asymptotic states". English. In: *Acta Geotechnica* 8.5 (2013), pp. 481–496.

[14] A. Niemunis and I. Herle. "Hypoplastic model for cohesionless soils with elastic strain range". In: *Mechanics of Cohesive-frictional Materials* 2.4 (Oct. 1997), pp. 279–299.

[15] Anamitra Roy et al. "Use of a bounding surface model in predicting element tests and capacity in boundary value problems". In: *Canadian Geotechnical Journal* (July 2020).

[16] P. Staubach and J. Machaček. "Influence of relative acceleration in saturated sand: Analytical approach and simulation of vibratory pile driving tests". In: *Computers and Geotechnics* 112 (Aug. 2019), pp. 173–184.

[17] P. Staubach et al. "Back-analysis of model tests on piles in sand subjected to long-term lateral cyclic loading: Impact of the pile installation and application of the HCA model". In: *Computers and Geotechnics* 134 (2021), p. 104018.

[18] P. Staubach et al. "Vibratory pile driving in water-saturated sand: back-analysis of model tests using a hydro-mechanically coupled CEL method". In: *Soils & Foundations* (2020).

[19] M. Tafili, W. Fuentes, and Th. Triantafyllidis. "A comparative study of different model families for the constitutive simulation of viscous clays". In: *Int J Numer Anal Methods Geomech.* 44 (2020). DOI: 10.1002/nag.3024, pp. 633–667.

[20] Jakob Vogelsang. "Untersuchungen zu den Mechanismen der Pfahlrammung". PhD thesis. Veröffentlichung des Instituts für Bodenmechanik und Felsmechanik am Karlsruher Institut für Technologie (KIT), Heft 182, 2017.

[21] T. Wichtmann, W. Fuentes, and T. Triantafyllidis. "Inspection of three sophisticated constitutive models based on monotonic and cyclic tests on fine sand: Hypoplasticity vs. Sanisand vs. ISA". In: *Soil Dynamics and Earthquake Engineering* 124 (Sept. 2019), pp. 172–183.

[22] P. Wriggers. *Computational Contact Mechanics*. Springer Berlin Heidelberg, 2006.

[23] O. C. Zienkiewicz, C. T. Chang, and P. Bettess. "Drained, undrained, consolidating and dynamic behaviour assumptions in soils". In: *Géotechnique* 30.4 (Dec. 1980), pp. 385–395.